SPECTROSCOPIC IMAGING OF EFFLUENT GASES

Diploma Paper

by

Pär Ragnarson

Lund Reports on Atomic Physics, LRAP-83

Lund, February 1988

SPECTROSCOPIC IMAGING OF EFFLUENT GASES

Diploma Paper

by

Pär Ragnarson

Instructor Ph. D. Hans Edner

CONTENTS PAGE

I. Abstract 3

II. Introduction 4

III. Theory 6

IV. Computer simulations 11

V. System description 14

VI. Results 15
i) Sulphur dioxide SO_2 17
ii) Nitrogen dioxide NO_2 18
iii) Plume measurement 19

VII. Estimation of error 20
Improvements 22

VIII. Acknowledgements 24

XI. Figure captions 25

X. References 28

ABSTRACT

This paper investigates the possibilites of imaging effluent gases in the atmosphere, using a passiv gas-correlation technique in the UV and visible region. The experiments have been focused on SO_2 but some measurements of NO_2 have also been carried out.

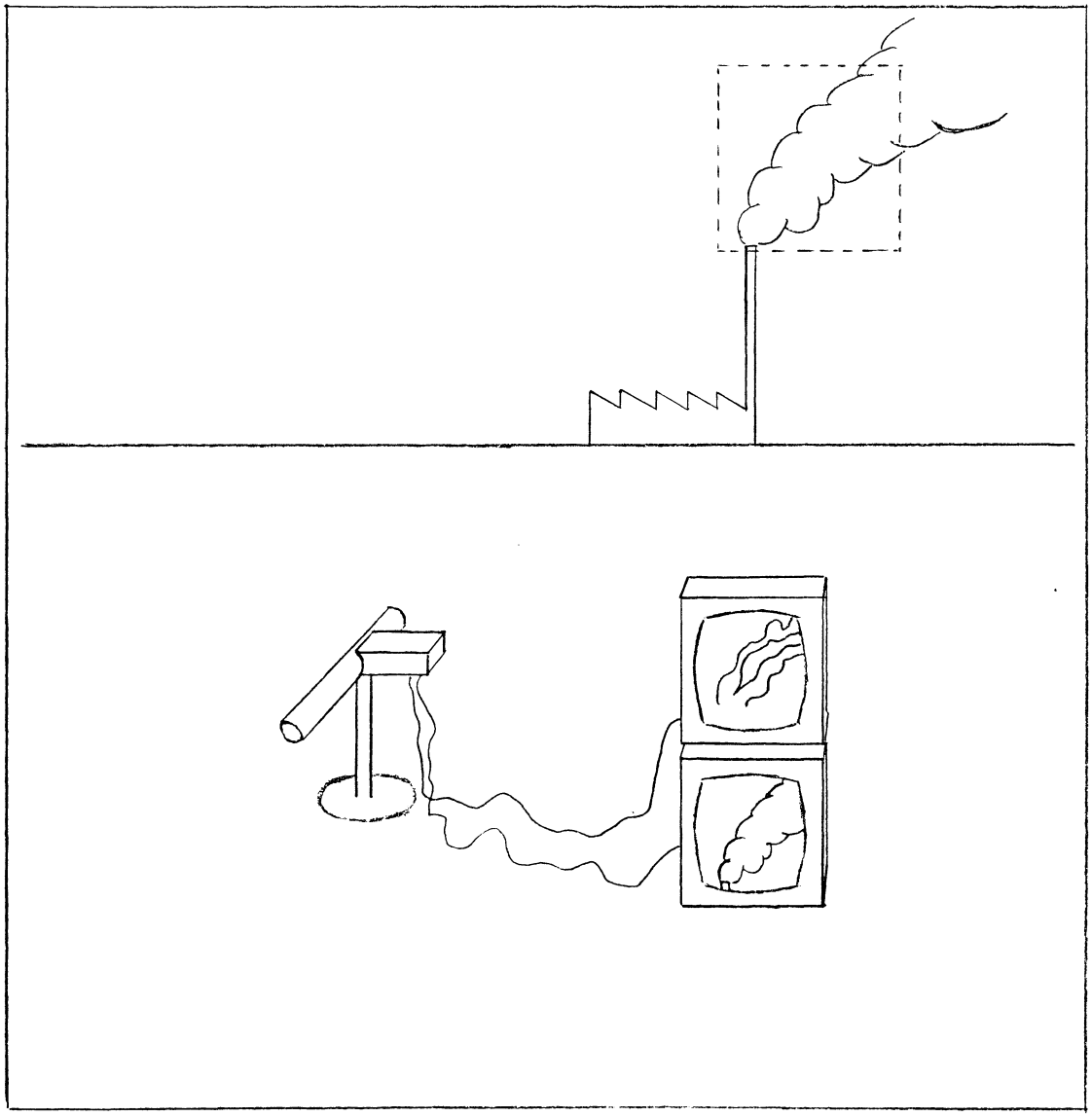

INTRODUCTION

The interest in measuring species in the atmosphere has increased as the environmental aspects have been given higher priority. Traditionally, stationary and chemical analysis methods have been used but the evolution of optical remote monitoring methods based on absorption spectroscopy provide new possibilities, especially when large regional mapping is required. A distinction can be made between active and passive remote-sensing instruments where the active ones use different types of artificial light sources such as classical lamps or lasers. Passive instruments use natural sources of radiation, normally the sunlight, scattered in the atmosphere or reflected against the earth. Numerous different instruments measuring path-averaged concentrations of pollutants have been developed e.g. DOAS (Differential Optical Absorption Spectroscopy) [1,2], Fourier Transform spectroscopy [3,4], optical filter systems [5], and dispersive correlation spectroscopy e.g. COSPEC [6]. Normally, the gas-correlation technique have been used in such path-averaged measurements [4,6-12]. The most powerful tools in remote atmospheric monitoring are based on the LIDAR technique (Light Detection And Ranging) with its range resolved measurements and possibility of 3-D mapping, and the techniques of LIDAR and gas-correlation have been combined as well [13].

The basic gas-correlation technique is nondispersive and all wavelengths are present at the detector making it fully multiplexed. The fundamental advantage compared to many other spectroscopic methods is the simplicity in handling. A gas-cell filled with the gas to be detected, is used as a matched spectral filter to identify the gas in a mixture of gases and the gas itself is therefore active in the discrimination against interfering gases. Gas-correlation technique have the advantage of working with dimensionless ratios. The benefit of forming dimensionless ratios is that the geometrical factors are eliminated and have no effect on the signal.

It is sometimes convenient to have an instant two-dimensionell image of the effluent gases. Due to limitation in dimensions, instrumens using dispersive components are often inappropriate, but the

nondispersive gas correlation technique could be a successful methode to use.

The present system uses a 1-D diode array detector but the extension to a 2-D matrix detector is obvious. The final image could be presented using false-colour-technique presenting the gasplume only, together with a normal black and white TV monitor to display the gas in its proper environment.

The plume mapping capability is valuable even if concentrations are not evaluated.

THEORY

The gas-correlation technique was demonstrated for the first time by K.F. Luft in 1943 as a nondispersive analyser [14]. The technique can be described with reference to Fig. 1. The region to be measured, which can be a gas cell, a chimney or the open atmosphere, is represented by an external cell, here called the target cell.

The signal from light directly reaching a detector is compared to the signal from light passing a cell filled with the gas species to be investigated. The filled cell, the correlation cell, has an optical depth (conc * length) that gives almost total absorption at the absorption peaks but light in between passes through. The direct channel is attenuated to the same level as the correlation cannel so that the ratio between the two channels becomes unity when there is no studied gas in the target cell.

Fig. 1

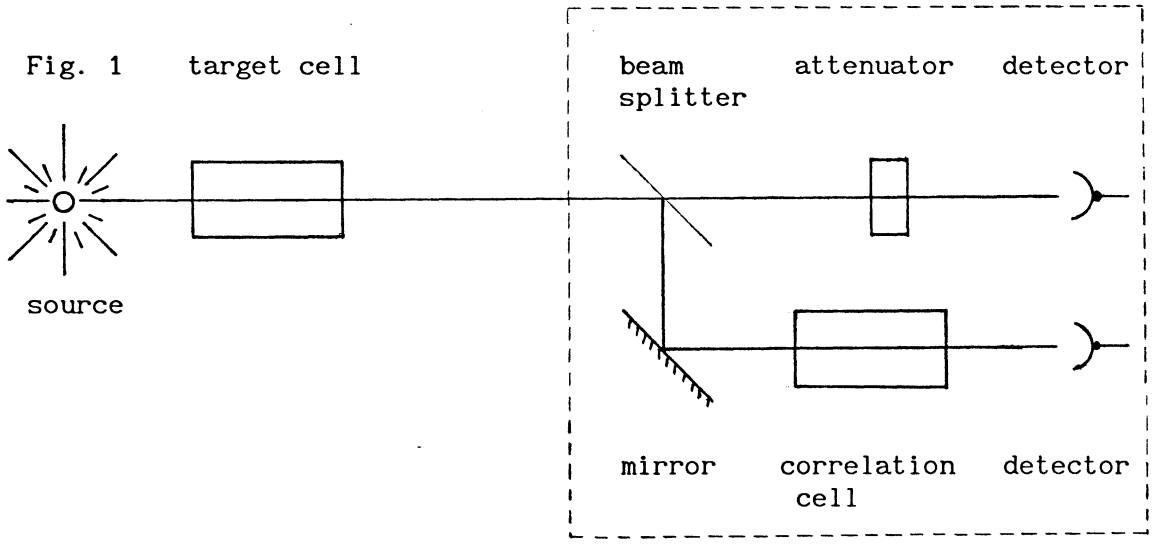

If the gas under study appears in the target cell, the absorption here will have little effect on the amount of light after the correlation cell, because the light absorbed in the target cell would not have passed the correlation cell anyway, and the detector could not tell whether the light was absorbed in front of or within the correlation cell. A decrease is observed in the direct channel and the imbalance increases with the amount of studied gas in the target cell.

The principle of gas-correlation is illustrated by the simplified transmission spectra drawn in Fig. 2a-c.

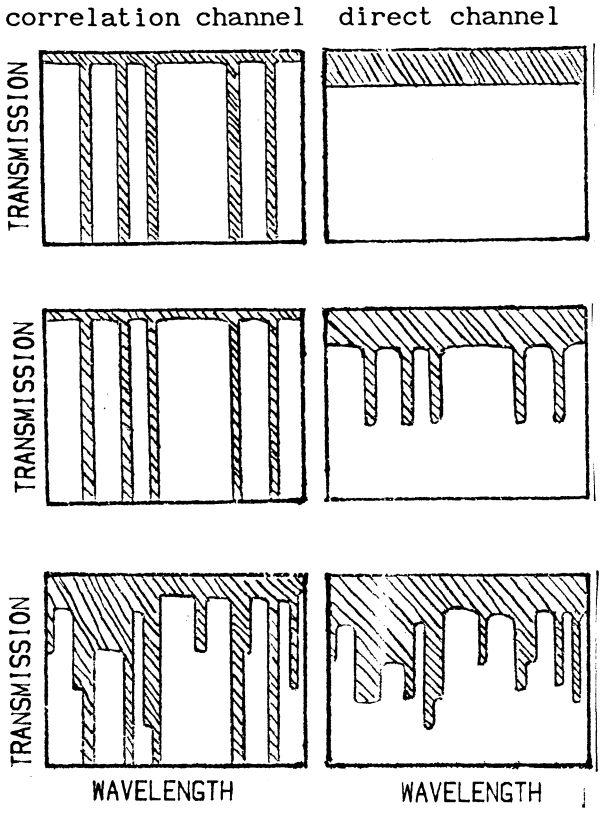

Fig. 2a

The direct channel is adjusted to transmit the same total intensity as the correlation channel.

Fig. 2b

If the light reaching the instrument contains absorption lines matching the gas in the correlation cell, these will only effect the direct cannel.

Fig. 2c

Interfering gases will generally attenuate the two channels equally and will therefore not effect the ratio between them.

This is true for every pair of corresponding pixels on the detector which makes the gas-correlation technique perfect for imaging applications.

The attenuation of the direct channel could be achieved by filling a similar cell with a continuum absorbing gas. An easier and therefore more common way is to use a neutral filter or a diaphragm aperture, alternatively adjust the detector electronically. The channels could also be adjusted in the signal processing and especially if an image-generating detector arrangement is used it is normally necessary to apply a function that compensates for detector nonuniformities and geometrical factors. The dimensionless ratio between the direct signal and the correlation signal, here called q, is compared to the ratio q_0 between the channels when the target cell is void of the studied gas. In the imaging detector arrangement, q_0 is a function of position, and in point measurements it is a number. The signal of interest is the relative decrease which can be written $Q = 1 - q/q_0$. In this paper it is refered to as the correlation signal. The beauty with gas-correlation technique is that the dimensionless ratio is insensitive to interfering gases with uncorrelated absorption spectra. However, two spectra have generally some correlation and there are two ways in

trying to filter out a spectral interval over which this unwanted correlation is minimized:

1) A sufficiently wide interval is chosen where the positive and negative contributions compensate each other. However, the signal may be reduced by including regions of less prominent absorption.

2) A sufficiently small interval, comprising the wanted spectrum, is is chosen. The risk is that the detected light could be so small that the signal could vanish in the noise. Many small intervals could be used for point measurements using dispersive methods [10].

In a mathematical description, the filtered spectral distribution is denoted by $S(\lambda)$, the transmission through the target cell $T_t(\lambda)$ and through the correlation cell $T_c(\lambda)$. Possible attenuation in the direct channel is denoted $A(\lambda)$ and is assumed to have approximately constant transmittance within the spectral interval under investigation.

$$I_{direct} = \int S(\lambda)T_t(\lambda)A(\lambda)d\lambda$$

$$I_{corr} = \int S(\lambda)T_t(\lambda)T_c(\lambda)d\lambda$$

The ratio between the signals, $q = \dfrac{I_{direct}}{I_{corr}}$

and in the same way $$q_0 = \frac{\int S(\lambda)A(\lambda)d\lambda}{\int S(\lambda)T_t(\lambda)d\lambda}$$

Neither $T_t(\lambda)$ nor $T_c(\lambda)$ are correlated with $S(\lambda)$ or $A(\lambda)$ so the latter ones could be eliminated in the quotient q/q_0.

The result is $$q/q_0 = \frac{\int T_t(\lambda)d\lambda \int T_c(\lambda)d\lambda}{\int T_t(\lambda)T_c(\lambda)d\lambda}$$

The correlation signal is now only dependent upon the correlation between the gases in the two cells. The correlation is positive if the absorption line of an interfering gas falls on top of one of the absorption lines of the target gas. The correlation signal will then

become larger than it would have been without interference. If the line falls between two absorption lines the correlation is negative and the correlation signal becomes smaller. A more detailed discussion of the gas-correlation technique can be found in Ref. 11.

The usefulness of a system is often dependent of the stability and reliability of the null balancing. If it is impossible to have the common path free from the gas to be detected, it may be difficult to calibrate for the true values of the measured concentrations. Atmospheric monitoring often means that only pollutants added to a background can be measured.

There are two different types of operation for gas-correlation systems

simultaneous measurement of the two channels or

alternating measurement.

The alternating type has two potential problems. If working in the IR region where the majority of the gaseous pollutants have their most characteristic signatures, the first obstacle to overcome is the thermal instability inside and outside the instrument, but the major drawback at all regions is that the light conditions could change between the measurements due to

1) fluctuations in the light source.
2) platform movements inducing swift background changes.
3) atmospheric turbulence.

The optical depth of the gas in the correlation cell is chosen for an optimum of discrimination and to maximize the product of the correlation signal and the average transmission through the correlation cell. If the optical depth is too small the difference between the channels decreases and so does the signal and detector noise could then become a problem. If it is too great, the amount of light decreases with increasing noise as a result. A high concentration cause a decrease in discrimination against other gases, because the broadened lines lead to a decrease in the influence from external absorption. As a rule of thumb, the gas should be essentially opaque at the strongest absorption lines [4,10,11]. The computer simulations (see below) indicate that an optical depth of 1300 ppm*m is optimal when operating with SO_2 in a region around 300 nm.

The discrimination is improved the more structured and detailed the spectrum is and therefore the system often becomes more efficient if the pressure in the correlation cell is reduced. The main structure will of course be intact but, since the correlation cell spectrum is more resolved, the detector will be able to see details in the transmission spectrum from the pressure broadened gases in the target cell. The disadvantage is that the absorption in the target cell will have greater effect on the correlation channel and the sensitivity will decrease.

A further step in improving the discrimination is to attenuate the direct channel using a gas-correlation cell containing the studied gas at high pressure (and therefore a shorter cell). The detection process is now to compare the absorption in the wings in the high-pressure cell to the absorption in the line centres in the low-pressure cell. The spectral region between the spectral lines will then have no effect on the measurements. The sensitivity will decrease in this arrangement as well [11,14].

COMPUTER SIMULATIONS

The intensity I reaching the detector after absorption in a gas is given by the Beer-Lambert law:

$$I = I_0 \exp(-\sigma c l), \quad \text{with}$$

I = light intensity after gas absorption
I_0 = light intensity without absorption
σ = absorption cross section of the gas
c = concentration of gas
l = absorption path length

The basis for the calculations performed was a spectroscopic measurement of SO_2 through a cell of known concentration (1700 ppm) and length (10 cm). This signal was compared with theoretical data and corrected to yield I/I_0 and the result is shown in Fig. 3. With the product $\sigma l = (\ln I/I_0)/c$, evaluated pixel by pixel, relative signals for other concentrations in the same cell could be evaluated: $I_x/I_0 = \exp(-\sigma l c_x)$. For example, Fig. 4 shows a processed transmission spectrum of a cell with the optical depth 1300 ppm*m.

$$\text{The ratio } q = \frac{\int \exp(-\sigma l c_c) d\lambda}{\int \exp(-\sigma l (c_x + c_{corr})) d\lambda}$$

$$\text{and } q_0 = \frac{1}{\int \exp(-\sigma l c_{corr}) d\lambda}$$

Concerning passive monitoring it is important to notice how drastically the amount of light available (the spectral irradiance) here called $E(\lambda)$, changes in the mid UV region (see Fig. 5) and a function was formed to describe this (see Fig. 6). The function is probably not strictly correct but hopefully it could illustrate the relative changes between the different wavelengths. The spectral region used in the measurements and in these simulations is formed by an interference filter centred to 299 nm with the halfwidth of 4.8 nm (see Fig. 7).

With the help of a simple program, the theoretical correlation signals $Q = 1 - q/q_0$ was evaluated for different concentrations of SO_2 at atmospheric pressure in the target- and correlation cell (Diagram I). By integrating the spectral distribution transmitted through the correlation cell, the total amount of light, here called <E>, was investigated for different concentrations in the correlation cell in order to be able to optimize the optical depth. In this spectral region the quality of the signal is limited by the shot-noise and the photons reaching the detector could be considered to be Poisson distributed. Then the photon noise is inversely proportional to the square root of the amount of light. The product $P = Q * \sqrt{<E>}$, constituting a quality factor for the system is calculated for different concentrations in the cells, though these simulations could not include variations in ability of discrimination. It was found that 1300 ppm*m is the optimum optical depth. Diagram II shows this product as a function of ppm*m.

To find out what could be gained if the filter was moved to an interval with more light but less prominent absorption, Diagram III was drawn showing how P, Q and $\sqrt{<E>}$ varies with the centre wavelength CW, (transmission T=0.38 and halfwidth BW=4.8 nm). Figure 7 shows one measured and one assumed filter profile. The latter, centred to 304 nm was used to evaluate the last values in Diagram III.
The question whether it is better to broaden the filter than to move the interval to longer wavelengths depends on the transmission of the filters used. For example, a filter at 302 nm with BW=4.8 nm and T=0.37 corresponds to a broader filter, BW=9.0 nm, at 299 nm if the transmission is 0.30. Diagram III is probably not to be trusted for higher values than about 302.5 nm. The spectrum of SO_2 was only known to 309 nm and the solar spectrum used is only approximate. Due to the shape of the solar spectrum in this spectral region, the true solar spectrum could change from day to day depending of the weather and the present state of the ozone layer. The most fundamental element to cause uncertainty in Diagram III is the problem when the filter profile is moved so far to the right that it reaches points outside the stored spectra. Even if the filter enables only a few percent of the intensity outside the known region to pass, the solar spectrum tells that this region is so strong it could in reality be dominant

when it is ignored in these simulations. The differential absorption is smaller here (see Fig. 8) and a more accurate study should probably show that the curve showing the evaluation of Q, would decrease faster and the product P could have a maximum within the spectral interval.

SYSTEM DESCRIPTION

Fig. 9 illustrates our present system. The sky radiation to be measured is collected with a Newtonian telescope. To divide the image into two identical images, a Cassegrainian telescope arrangement with a split primary mirror, originally constructed for medical fluorescence imaging [18], was used. One of the images passes through the correlation cell (100 mm long and a diameter of 25 mm) located in front of one of the entrances of the Cassegrainian telescope (see Fig. 10).

The unique components in this system are the four segmented mirrors in the Cassegrainian arrangement. The individually adjustable mirror segments allow the images to be placed side by side on the linear detector. The arrangement is shown in Figure 11. In this experiment only two mirrors were used and the filters were placed in front of the detector. No attenuator was used in the SO_2 measurements but a diaphragm was used measuring NO_2. The image-resolving Cassegrainian telescope is designed to look at objects at a short distance (about half a metre) so it is often necessary to have it matched to a light collecting telescope providing a picture of the area to be investigated. In this experiment a Newtonian telescope with a 25 cm primary mirror and a focal length of 100 cm was used.

The detector is a commercial image-intensified linear diode array model 1421 in a EG&G OMA III optical multichannel system. A small cell, 10 mm long, was placed in front of the image-plane of the Newtonian telescope to be used as a target cell. The cell was connected to a vacuum system and a six- litre glass bulb used as a mixing volume for concentrated gas and air. This cell was used to simulate an external SO_2 plume but was fully controllable. In the measurements on SO_2 a narrow band interference filter with T=0.38, CW=299.1 nm and BW=4.8 nm plus a SCHOTT UG11 coloured glass filter were used. The total integration time for every signal was twenty seconds (20 read-outs * 1 second integration time each). The NO2 measurements were performed with an interference filter with T=0.73, CW=447.5 nm and BW=5.0 nm. The total integration time was 20 seconds (1200 * 16.67 milliseconds).

RESULTS

The Newtonian telescope was aimed at the sky to collect scattered sunlight. The measurements on SO_2 suffered from poor irradiance and the quality of the correlation signals was rather weather dependent. Data from the detection unit are shown in Figs. 12-21, the background has been subtracted from all signals. The two images on the linear array appear on the OMA-display where the x-axes tell the position of the pixel on the detector and the y-value gives the intensity at that position. The Figures 12-13 and 16-17 are divided into four parts, numbered I to IV. Number I and II cover the image which has passed through the correlation cell and Number III and IV cover the image of the direct channel. The small cell, simulating a plume, was placed to cover half the image from the Newtonian telescope and Number I and III are the parts of the images that have passed through the target cell. The shapes of the correlation image and the direct image are very different as well as their total intensity, but by forming dimensionless quotients this is no fundamental problem if the noise-level is under control. The differences are due to vignetting, light leakage at the edge of the filter, detector nonuniformities, angular imperfections and other geometrical factors, especially when the target cell is used (compare Fig. 12 showing signals taken with the target cell to Fig. 19 showing signals without the cell). In the signal processing, the two channels were balanced by dividing the measured signal with a mean value of signals obtained with vacuum in the target cell. In a measurement with the target cell evacuated, a so called null measurement, the theory says that the two images from the balanced detector should be identical, that is a straight line at unity and this line could be seen as the reference level from which the decrease should be measured. The curve B in Fig. 13 shows an experimental result when SO_2 was in the correlation cell. If there is gas in the target cell, the result should be (according to the theory) that the level of the part of the balanced detector that is effected by the target cell, should decrease more in the direct channel than in the correlation channel. This is also born out in the experimental results, see e.g. curve A in Fig. 13.

It was mentioned above that the final correlation signal is achieved as $1 - q/q_0$. In the measurements however, the reference level usually had a value differing from one. This is a result of fluctuations in the intensity level due to metrologic conditions and the position of the sun. It is easily taken care of in the signal processing, so that the decrease is normalized to this level.

When two signals from the detector are divided with each other, the resulting curve could partly be very noisy. Take Fig. 12 for example, all the information is in the correlation image and the direct image, and outside these regions (to the left of part I, between part II and III, and to the right of part IV) the curves contain only noise (part IV is troubled with a light leakage which makes it very sensible to fluctuations at all wavelengths). The result, noise divided with noise, will of course be increased noise. It should be stressed that the resolution is not effected by limitations in the OMA system when the two signals are divided with each other. To improve readability the uninteresting parts of the curves are rejected in many figures.

SULPHUR DIOXIDE SO_2

The concentration of SO_2 in the correlation cell during these measurements was approximately 1000 ppm*m and the total pressure was 40 torr. Fig. 12 shows the signal when the target cell is evacuated, a signal from now on called the vacuum signal, and the signal when the target cell has a certain optical depth, and therefore called the gas signal. In this case the optical depth was 600 ppm*m. Following the theory, the distinction between the signals is that the decrease due to absorption in the target cell, is larger in part III than in part I. The two curves are almost identical in part II and IV. The gas signal divided with the vacuum signal results in curve A, in Fig. 13. It could be compared with curve B, which is two vacuum signals divided with each other and therefore illustrating the null signal from a signal-adjusted detector when there is no absorbing gas present in the target cell. It can be clearly seen, that the left part (the correlation image) is noisier which is due to the lower light intensity (a lot of light is absorbed in the correlation cell compared to the direct channel having no attenuator).
To see how much more the intensity dropped in the direct channel compared to the correlation channel, the right (direct-) image of curve a is divided with the left (correlation image) of the same curve. The result is q/q_0 which could be seen to the left in Fig. 14. Since we are interested in imaging the gas only, the final signal Q is received as $Q = 1 - q/q_0$ and it is shown to the right in Fig. 14.

Diagram IV shows the result of measurements with different concentrations in the target cell. The curve is a calculated one, taken from Diagram I, corresponding to the optical depth of 650 ppm*m (50 torr*cm). The standard error in the correlation signal from a number of null-measurements was 0.02 and it corresponds to an uncertainty in the correlation signal of 85 ppm*m.

NITROGEN DIOXIDE NO_2

The differential absorption is considerably smaller for NO_2 (see Fig. 15) compared to SO_2 but the irradiance in the used interval (around 450 nm) is tremendously much higher (see Fig 5). The result is a smaller but less noisy correlation signal.

In this measurement the correlation cell contained approximately 3300 ppm*m at a total pressure of 150 torr.

The vacuum curve and the signal when the target cell contained approximately 1500 ppm*m is shown in Fig. 16. The gas curve divided with the vacuum curve is shown in Fig. 17 where it is called curve A, for comparison a null signal (curve B) is also drawn in this Figure. The ratio q/q_0 and the final correlation signal are shown in Fig. 18. In this wavelength interval ($\simeq$442-453 nm) there is considerably more light for passive monitoring. The improved signal-to-noise ratio leads to a very low noise level. This is obvious by comparing the null signal in Fig. 17 to the one in Fig. 13. Since the concentrations of NO_2 could not be calibrated there are no figures of the standard deviation in these measurements.

PLUME MEASUREMENT

No measurement of a SO_2 plume were carried out since there was no suitable source to aim at from our laboratory. However, at a distance of 430 metres from the laboratory, there is a chimney of a combustion station but the plume did not contain SO_2. Instead the plume was used to study the influence of particle scattering.

Particles generally attenuate radiation equally within a small interval. To be more accurate, the attenuation due to Mie- and Rayleigh scattering has a monotonous wavelength dependence without sharp features, and the presence of particles will, just like an uncorrelated gas, reduce the two channels in the same proportion and leave the ratio between the two signals unaffected.

A problem connected to passive measurements of plumes is that light being reflected by particles before reaching the detector have not passed through the whole plume and therefore scattering could lead to a dilution of the signal and the measured correlation signal would indicate a concentration smaller than the true one.

At the measurement of the plume the pressure of SO_2 in the correlation cell was around 10 torr, no target cell was used. The measurement was performed at the edge of the plume where it reduced the amount of light by 10%. A sequence of figures (Fig. 19-21) show that the plume had no significant influence on the correlation signal.

ESTIMATION OF ERROR

A large source of error in the measurements is the fact that if was difficult to carefully handle gases at low pressure. At the data taking for diagram IV, the correlation cell was filled with a partial pressure of SO_2 to yield 7 torr but it could have been anything between 5 and 10 torr. According to the curve in diagram IV (taken from Diagram I) it was close to 5 torr but this curve was calculated for a correlation cell with gas of atmospheric pressure (If diagram IV is studied thoroughly, it could be suspected that the values are shifted to the right and that the corresponding curve should be steeper, indicating a higher concentration in the correlation cell). Although it is not likely that the spectral lines of SO_2 were fully resolved in this low pressure correlation cell, it is possible that the sensitivity would have increased if there had been atmospheric pressure in the cell. Since there are very few gases with interfering spectra in this interval there is hardly any reason trying to increase the selectivity at the expense of the sensitivity. The reason for the low pressure was only practical.

To be able to do the measurements that lead to diagram IV the glass-bulb was filled with approximately 10% pure SO_2 and the rest ordinary air. The target cell (1 cm long) was evacuated and then filled up from the bulb. The cell now contained 1000 ppm*m with an error of approximately 6% (in this case 60 ppm*m) and the next point was obtained by evacuating a small amount of the gas from the glass-bulb and replace it with air. After evacuating the target cell again, it was filled with the new mixture in the glass-bulb. Repeating this, the curve was obtained from the right to the left. In this process an error could be introduced between the successive values and this error could be estimated to be approximately 1%. For example, if the value 1000 ppm*m was correct, the error in the following value 940 ppm*m could be 10-15 ppm*m. The error accumulates in this process, so the error in the last point (140 ppm*m) could be 20% or 25-30 ppm*m. This error combined with the potential error of 60 ppm*m in the original concentration means that the total error in the value of the optical depth in the target cell could in the worst case be almost 100 ppm*m.

A problem arising from the arrangement with the target cell is that only half of the images are free from its disturbances. Due to the angular imperfections, the size of the edge of the target cell appears to be different for the correlation image and the direct image. Also, the fact that the target cell is not being in focus plus the vignetting in the correlation cell, have the effect that the two images do not have the same size and the division between the two could not be correct.

To be able to do the NO_2 measurement we mixed our own gas by filling the glass bulb with NO and air. The measurements carried out could only be considered to be exploratory and are just made to investigate the magnitude of the signal and the noise level.

Measuring SO_2, the standard error in correlation signal Q was found to be 0.02 which corresponds to 85 ppm*m. At 1000 ppm*m the correlation signal was 0.20 but according to Diagram I, with the optical depth of 1300 ppm*m it could theoretically be 0.30. In that case, the same noise level would cause an uncertainty in the correlation signal representing 50 ppm*m.
The Achilles' heel of this present system for measuring SO_2 is the low irradiance in the chosen bandpass. Diagram III shows that if the narrow-band filter is centred around 302 nm then four times as much light will be obtained while maintaining 80% of the correlation signal. In a measurement made with a filter centred to 316 nm, the signal was improved 47 times (but increasing from such a low intensity level that the quality of the signal is still considered to be limited by shot-noise) and at the same time the noise was reduced by a factor of 6. The correlation signal was much too small to be useful but 6 is very close to 7 ($\sqrt{47}\simeq 7$) so this measurement makes it probable that the noise could be cut to the half by centring the filter to 302 nm. A problem arising from photon limited signals is that the variations in the background radiation could make it impossible to use one single compensation function q_0. In the SO_2 measurements, the correlation signal was generally better when the vacuum-signal was updated for every obtained gas signal.

IMPROVEMENTS

The first improvement would be to double the diameter of the correlation cell. It would give this channel four times as much light. Advantage should be taken from the fact that the technique does not suffer from angular restrictions and the diameter of the correlation cell could be large without economical or technical difficulties. Furthermore, the fact that the gas-correlation technique is fully multiplexed gives the technique a large light gathering capability. Apart from the optical depth, the limitations are mainly due to interference filters and detectors.

SO_2 measurements would benefit from using a different filter to reduce the noise level.

To be able to use the system practically it is obviously necessary to have an automatic signal processing. It would then of course be much easier to set up the system and to compare theoretical to measured values.

Future studies would comprise field experiment to study the system performance in its proper environment. Laboratory studies of interference from other gases are yet to be done.

Evident developments are simultaneous measuring of different gases or improving the versatility and of course, proper 2-D imaging.

To be investigated is whether the system would become more accurate if e.g. two different correlation cells were used simultaneously. Possible advantages of multi-cell arrangements must be weighed against the decrease in spatial resolution since more images have to share the detector area. Especially if mean value averaging between pixels is necessary, a decrease in spatial resolution could be fatal.

Gas-correlation techniques could be used to detect a number of different species in the atmosphere. The efficiency is determined by the size of the differential absorption and the degree of interference from other gases. The spectral interval to be utilized is also dependent on the spectral distribution of the radiation source, the

absorption spectra of the atmosphere and technical considerations. Airborne downward viewing instruments also have to consider the distribution of the background radiation.

The investigations have shown that imaging of SO_2 should be possible. Minor changes would give half the noise-level and with an uncertainty of 50 ppm*m or less in measuring the atmospheric burden, it could hopefully be a useful instrument. The concentration in a SO_2-polluting plume normally contain several hundred ppm*m.

Detection of NO_2 should be feasible as well. The differential absorption is considerably smaller for NO_2 but the signal is a lot better then for SO_2. The concentration of NO_2 in a plume could be almost as high as the SO_2-burden.

ACKNOWLEDGEMENTS

The author is very grateful to everyone at the department of physics in Lund for all their help and understanding. I would especially like to thank Stefan Andersson-Engels and Jonas Johnsson in the medical group for their instructions of the Cassegrainian telescope and the OMA. Finally, I wish to thank my instructor, Ph.D. Hans Edner and Anders Sunesson in the LIDAR-group for all their efforts in making this project possible, and of course professor Sune Svanberg for allways being an endless sourse of inspiration.

FIGURE CAPTIONS

Fig. 1. Schematic arrangement of a basic gas-correlation spectrometer.

Fig. 2. Simplified transmission spectra of the two channels
a) with no external gas to detect
b) showing the effect of the specified gas in the common light path.
c) the effect of the specified gas together with interfering gases

Fig. 3. Spectroscopic measurement of SO_2, corrected to yield I/I_0 for 170 ppm*m.

Fig. 4. Processed SO_2 transmission spectrum through a cell with the optical depht of 1300 ppm*m.

Fig. 5. Solar spectrum at sea level, adopted from Ref. 17.

Fig. 6. Plot of an approximate distribution of the sunlight at sea-level, adopted from ref. 16.

Fig. 7. Measured filter profile (left) used in calculating theoretical output signals (diagram I) and the product P vs. concentration in the correlation cell (diagram II). The filter the right is a calculated Gaussian curve, simulating a filter to attain the last values in diagram III

Fig. 8. SO_2 absorption spectrum, from Ref. 18.

Fig. 9. Description of the present arrangement.

Fig. 10. Schematic details of the optical instrument in the arrangement.

Fig. 11. Cassegrainian optical system, constructed for one- or two-dimensional multi-colour imaging.

Fig. 12. Signals from the detector when the target cell was evacuated (the vacuum signal) and when it had the optical depth of 600

ppm*m SO_2 (the gas signal). In both cases, the correlation cell contained around 1000 ppm*m.

Fig. 13. Curve A, is the gas signal and the vacuum signal divided with each other, pixel by pixel. Curve B, is the ratio between two different vacuum curves and then representing a null signal from a balanced detector.

Fig. 14. The left curve is the dimensionless quotient q/q_0 achieved by dividing the right part of curve A in Fig. 13 with the left part. To the right is the final correlation signal Q formed by $Q = 1 - q/q_0$.

Fig. 15. NO_2 absorption spectrum, from Ref. 20.

Fig. 16. Signals with evacuated target cell, and when it was filled with 1500 ppm*m NO_2. The optical depth in the correlation cell was 3300 ppm*m.

Fig. 17. Curve A is the ratio between the gas- and vacuum curve above and curve B is two vacuum curves divided with each other.

Fig. 18. The dimensionless ratio q/q_0 to the left and to the right the correlation signal Q.

Fig. 19. Signal of "clean" air and the signal from looking at the edge of the plume.

Fig. 20. Plume-signal divided with "clean air"-signal.

Fig. 21. The ratio q/q_0 and the final correlation signal.

Diagram I. Calculated correlation signals measuring SO_2.

Diagram II. The relative product P: correlation signal Q times the square root of the intensity <E>, at different values of the optical depth in the correlation cell.

Diagram III. Correlation signal Q , the square root of the intensity <E>, and the product P vs. centre wavelength of a narrow band interference filter.

Diagram IV. Measured SO_2 correlation signals and the calculated calibration curve corresponding to the optical depth of 650 ppm*m.

REFERENCES

1) H. Edner, A. Sunesson, S. Svanberg, L. Unéus and S. Wallin, " Differential Optical Absorption Spectroscopy System used for Atmospheric Mercury Monitoring," Appl. Opt. **25**, 403 (1986).

2) U. Platt and D. Perner, Measurements of Atmospheric Gases by Long Path Differential UV/Visible Absorption Spectroscopy. in Optical and Laser remote Sensing, D. K. Killinger and A. Moordian, Eds., (Springer-Verlag, Heidelberg, 1983).

3) W. F. Herget and J. D. Brasher, "Remote Measurement of Gaseous Pollutant Concentrations Using a Mobile Fourier Transform Interferometer System," Appl. Opt. **18**. 3404 (1979).

4) A. Galais, G Furtunato and P. Chavel, "Gas Concentration Measurement by Spectral Correlation: Rejection of Interferent Species", Appl. Opt. **24**, 2127 (1985).

5) H. B. McElhoe and W.D. Conner, "Remote Measurements of Sulfur Dioxide Emissions Using an Ultraviolet Light Sensitive Video System", JAPCA. **36**, 42 (1986).

6) J. H. Davies, A. R. Barringer and R. Dick, "Gaseous Correlation Spectrometric Measurements", in Optical and Laser Remote Sensing, D. K. Killinger and A. Moordian, Eds. ,(Springer, Heidelberg, 1983).

7) H. S. Lee and H. H. Zwick, "Gas Filter Correlation Instrument for the Remote Sensing of Gas Leaks", Rev. Sci. Instrum. **56**, 1812 (1985).

8) R. Goody, "Cross-Correlating Spectrometer", J. Opt. Soc. Am. **58**, 900 (1968).

9) T. V. Ward and H. H. Zwick, "Gas Cell Correlation Spectrometer: GASPEC", Appl. Opt. **14**, 2896 (1975).

10) W. F. Herget, J. A. Jahnke, D. E. Burch and D. A. Gryvnak, "Infrared Gas-Filter Correlation Instrument for in situ Measurement of Gaseous Pollutant Concentrations", Appl. Opt. **15**, 1222 (1976).

11) D. E. Burch and D. A. Gryvnak, "Cross-Stack Measurement of Pollutant Concentrations Using Gas-Cell Correlation Spectroscopy", in Analytical Methods Applied to Air Pollutant Measurements, R. K. Stevens and W. F. Herget, Eds. (Ann Arbor Science Publishers, Ann Arbor, 1974); also EPA Report 650/2-74-094 (1974).

12) H. Edner, S. Montán, A. Sunesson, S. Svanberg, L Unéus, W. Wendt, "Active Remote Sensing of Atmospheric Pollution Using a Flashlamp-based Gas Correlation System, LRAP-83, (1987).

13) H. Edner, S. Svanberg, L Unéus and W. Wendt, "Gas-Correlation LIDAR", Opt. lett. **9**, 493 (1984).

14) K. F. Luft, "Über eine Neue Methode der Registrierenden Gasanalyse mit Hilfe der Absorption Ultraroter Strahlen ohne Spektrale Zerlegung," Z. Tech. Phys. **5**, 97 (1943).

15) Bendix Process Instruments Division, Ronceverte. W.Va.

16) F. Urbach and M.L. Wolbarsht, "Occupational Skin Hazards from Ultraviolet (UV) Exposures", SPIE, **279**, Ultraviolet and Vacuum Ultra Violet Systems, 201 (1981).

17) J. Bleckert, "Inledande Försök till Mätning av H_2O med Två Olika Raman-Lidar-System", LRAP-50, (1985).

18) J.D. Brassington, " Measurements of the SO_2 Absorption Spectrum Between 297 and 316 nm Using a Tunable Dye LASER", Laboratory note No. RD/L/N 184/79, Central Electricity Research Laboratories, Leatherhead, Surrey.

19) P. S. Andersson, S. Montán and S. Svanberg, "Multi Spectral System for Medical Fluorescence Imaging", J. Quantum Electronics, **23**, 1798, (1987).

20) N. Takeuchi, H. Shimizu and M. Okuda, "Detectivity Estimation of the DAS LIDAR for NO_2", Appl. Opt. **17**. 2734 (1978).

FIG. 3.

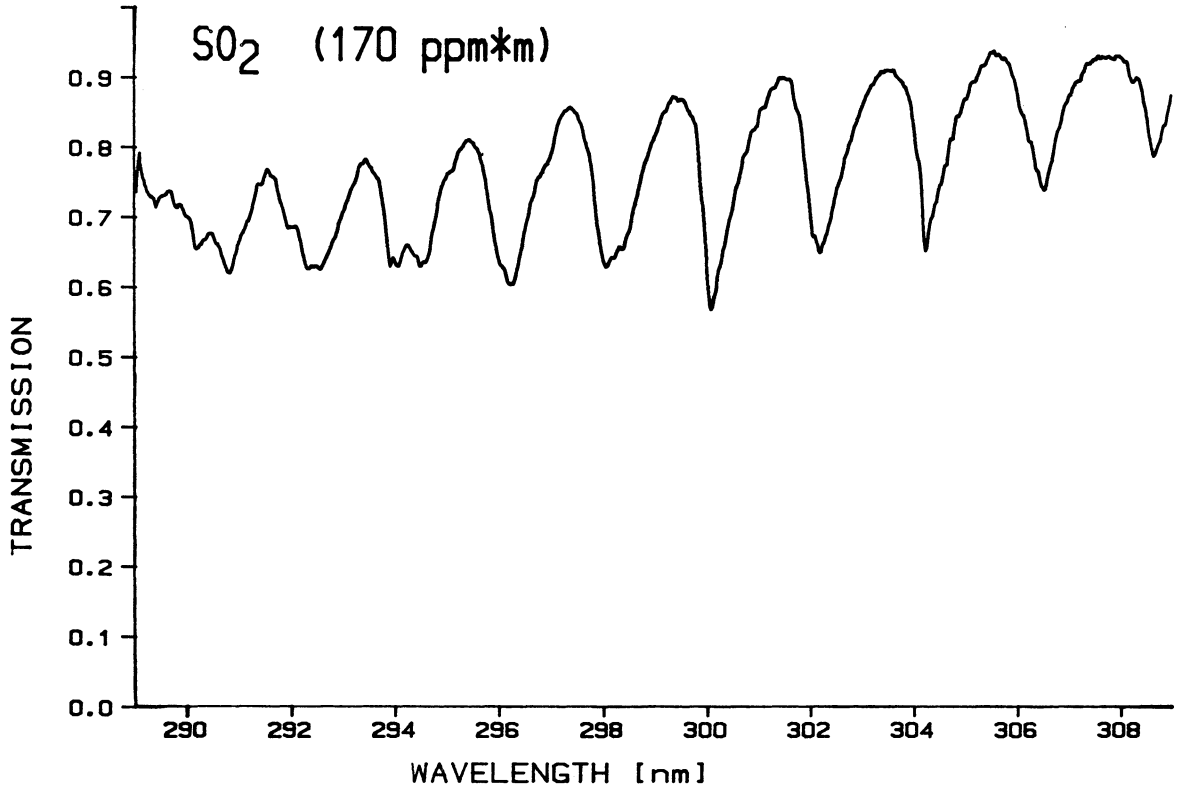
SO2 (170 ppm*m)
TRANSMISSION
0.0
0.1
0.2
0.3
0.4
0.5
0.6
0.7
0.8
0.9
290
292
294
296
298
300
302
304
306
308
WAVELENGTH [nm]

FIG. 4.

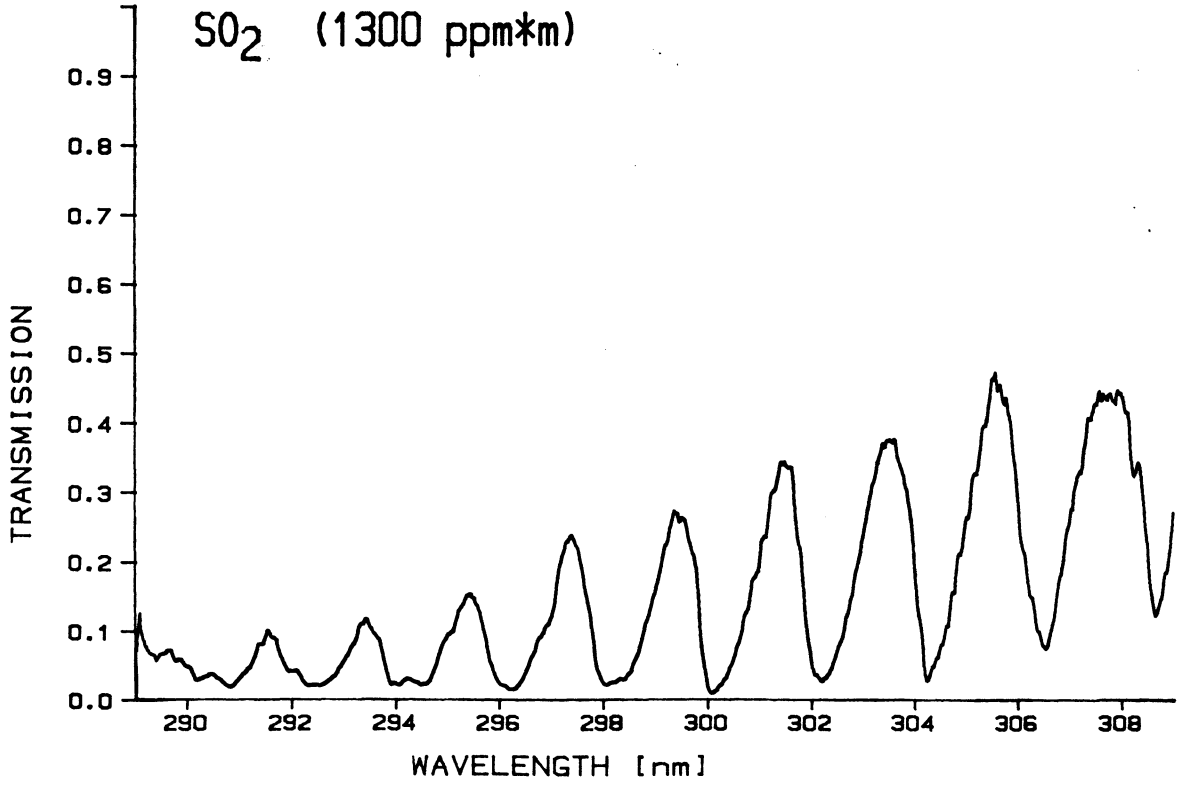
SO2 (1300 ppm*m)
TRANSMISSION
0.0
0.1
0.2
0.3
0.4
0.5
0.6
0.7
0.8
0.9
290
292
294
296
298
300
302
304
306
308
WAVELENGTH [nm]

FIG. 5.

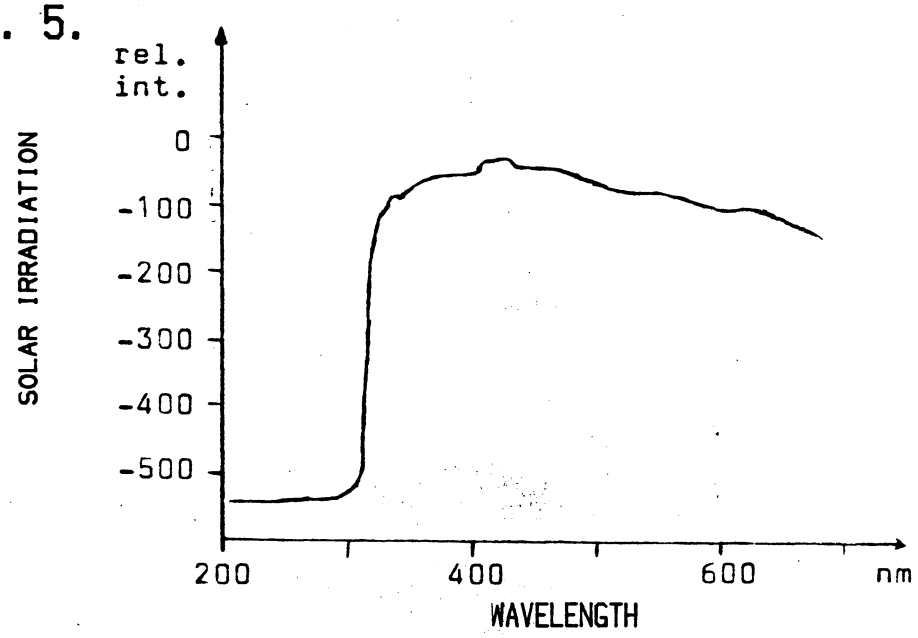

FIG. 6.

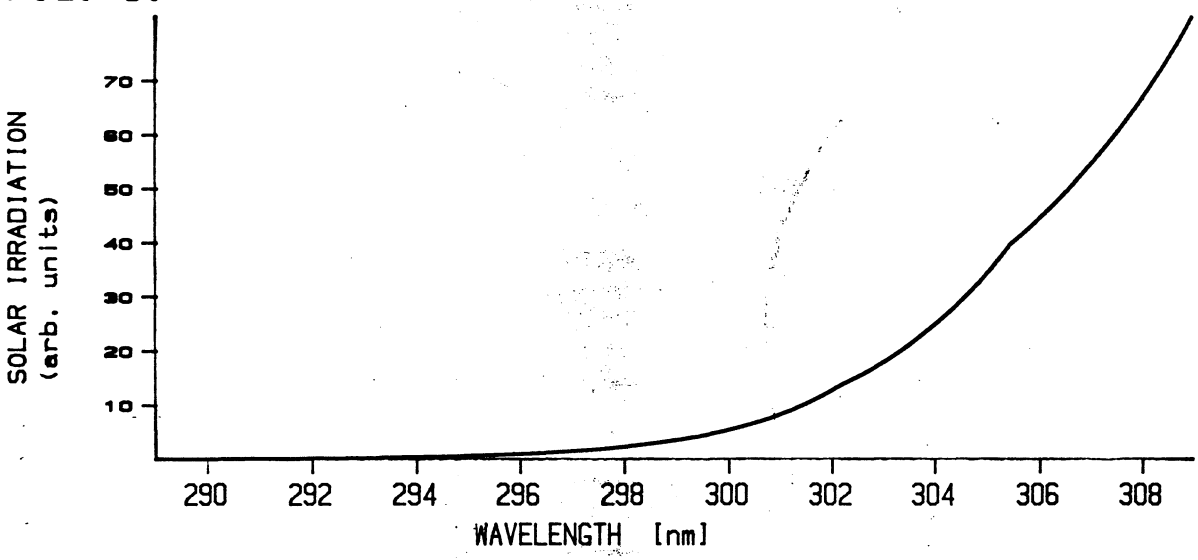

FIG. 7.

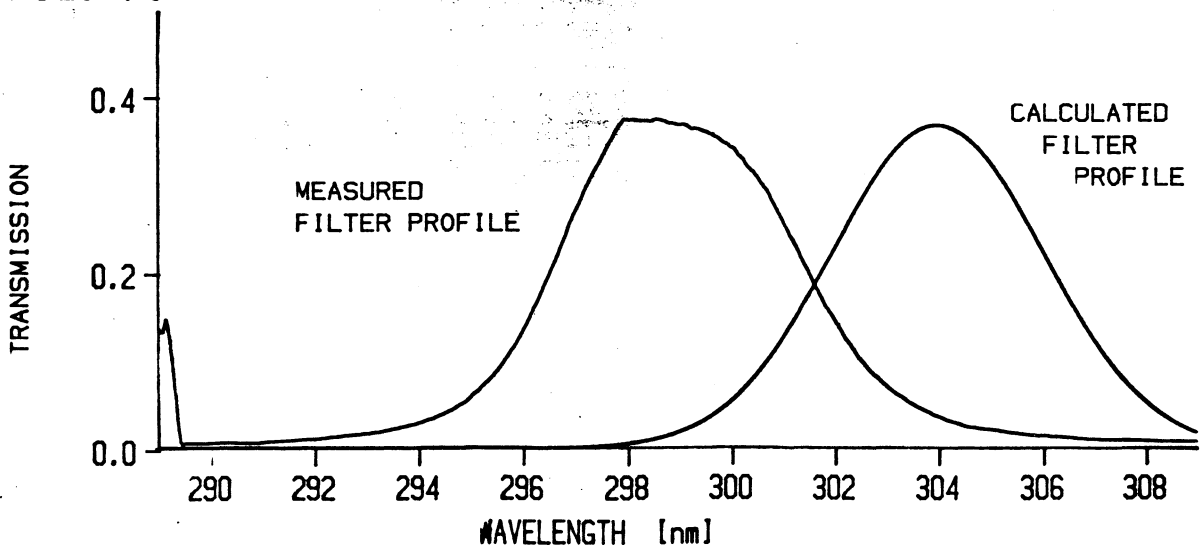

FIG. 8.
[Ref. 18]

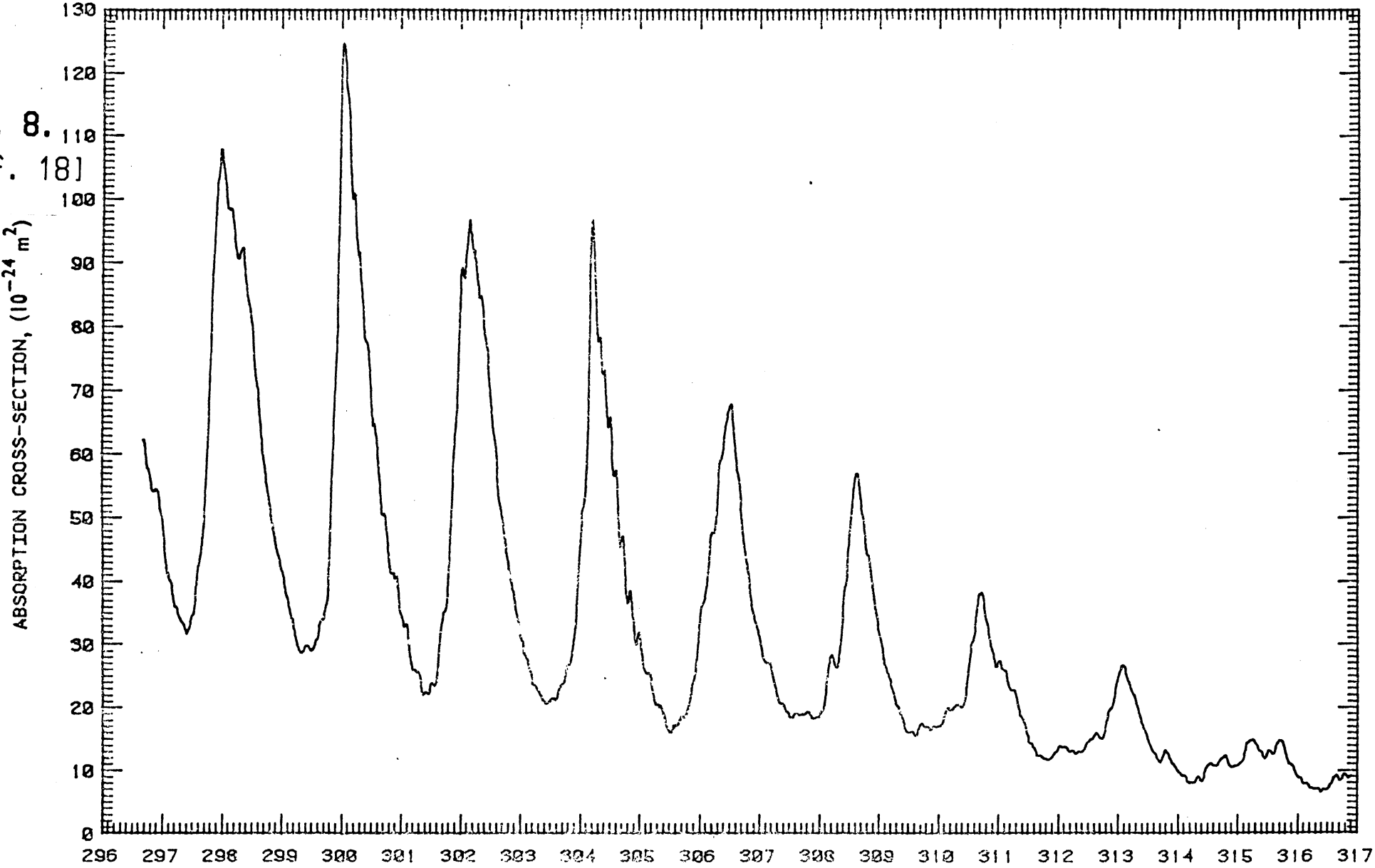

SO_2 ABSORPTION CROSS-SECTION AT 20°C FROM 296–317 nm

FIG. 9.

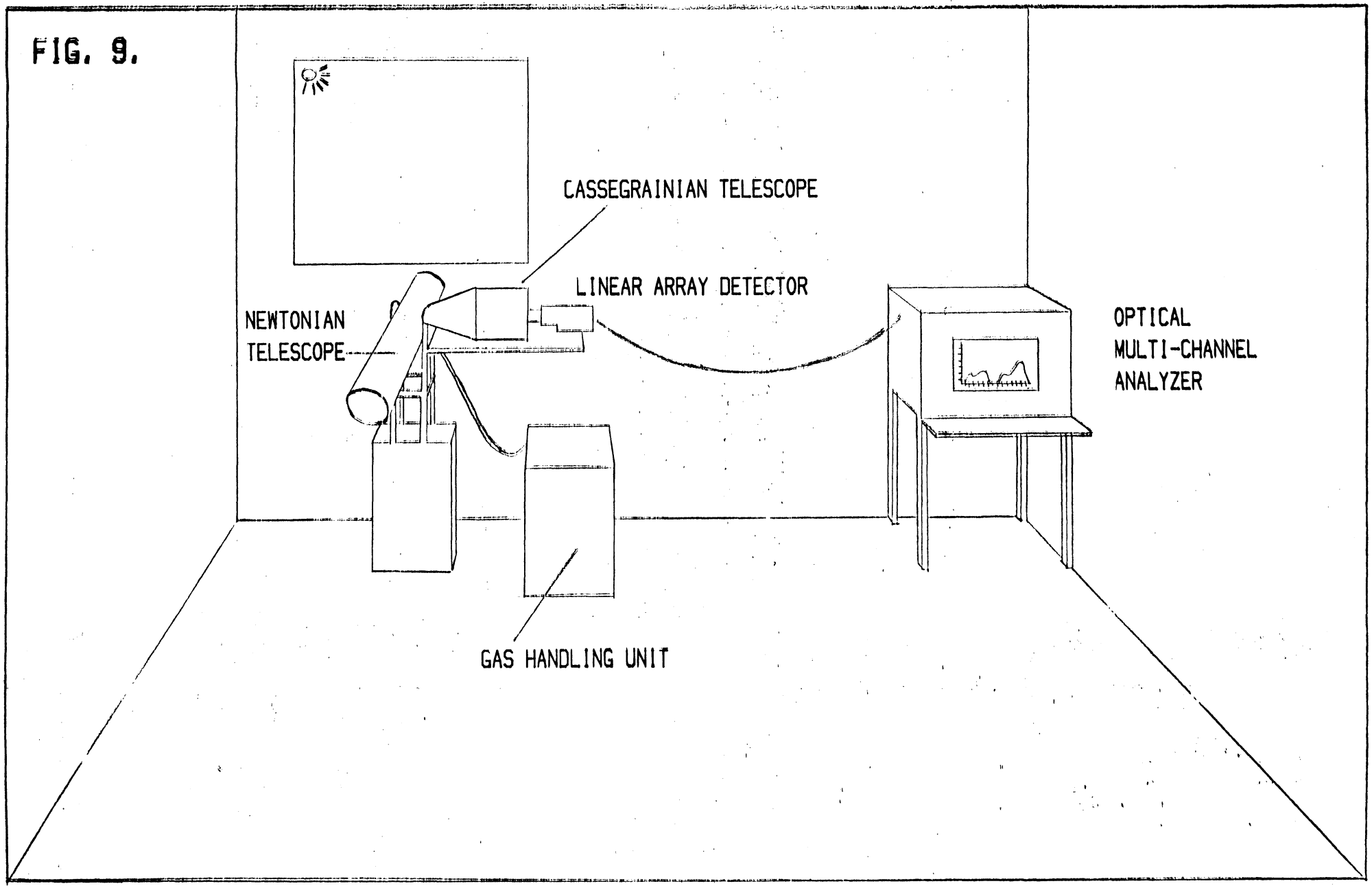
CASSEGRAINIAN TELESCOPE
LINEAR ARRAY DETECTOR
NEWTONIAN
TELESCOPE
OPTICAL
MULTI-CHANNEL
ANALYZER
GAS HANDLING UNIT

FIG. 10.

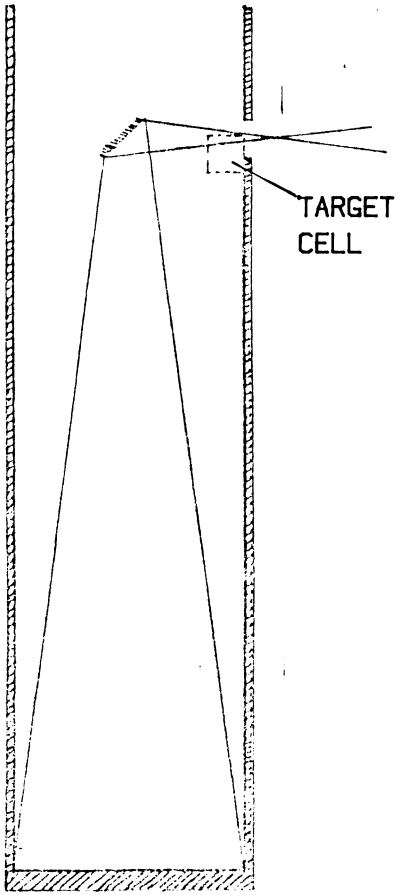

NEWTONIAN
TELESCOPE

CASSEGRAINIAN SYSTEM

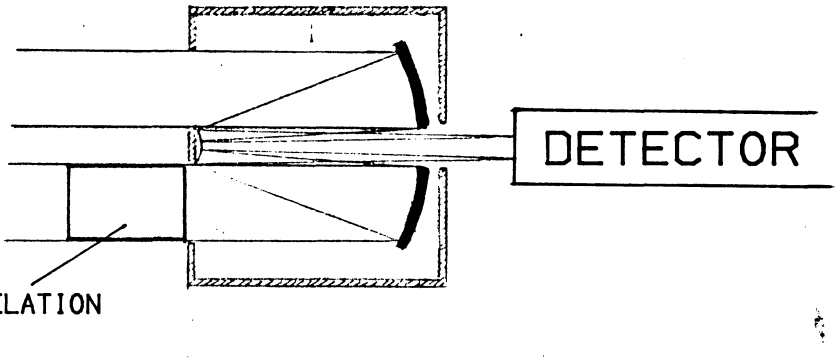

FIG. 11.

FRONT VIEW

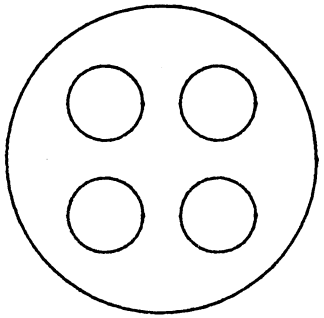

MIRROR ARRANGEMENT
(FRONT
VIEW)

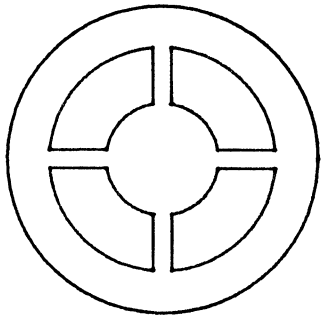

SO_2 MEASUREMENT

FIG. 12.

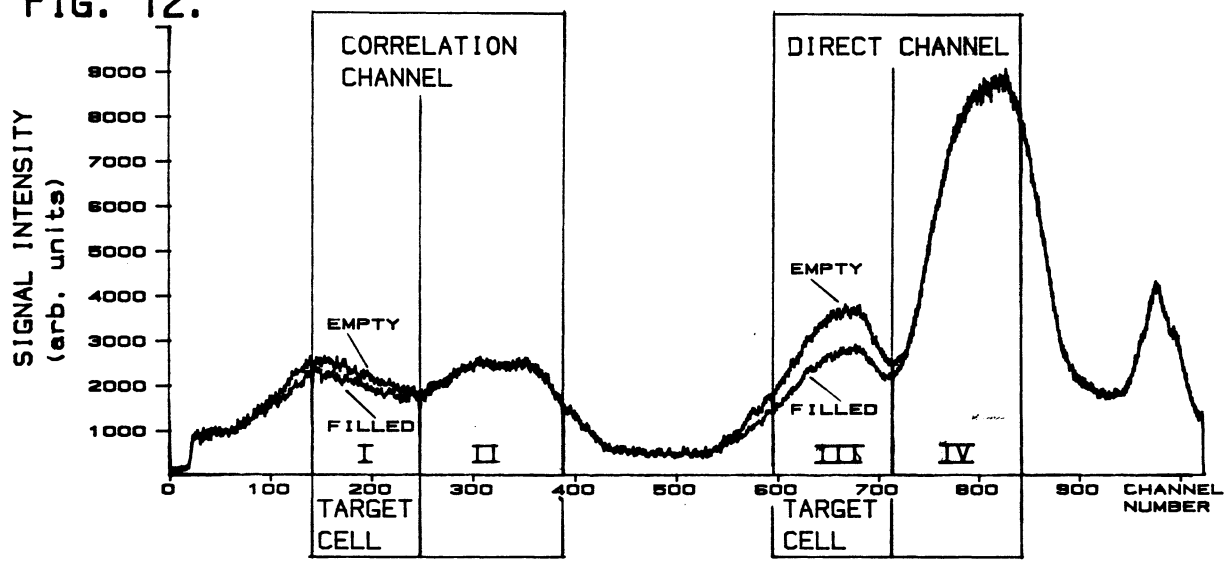

FIG. 13.

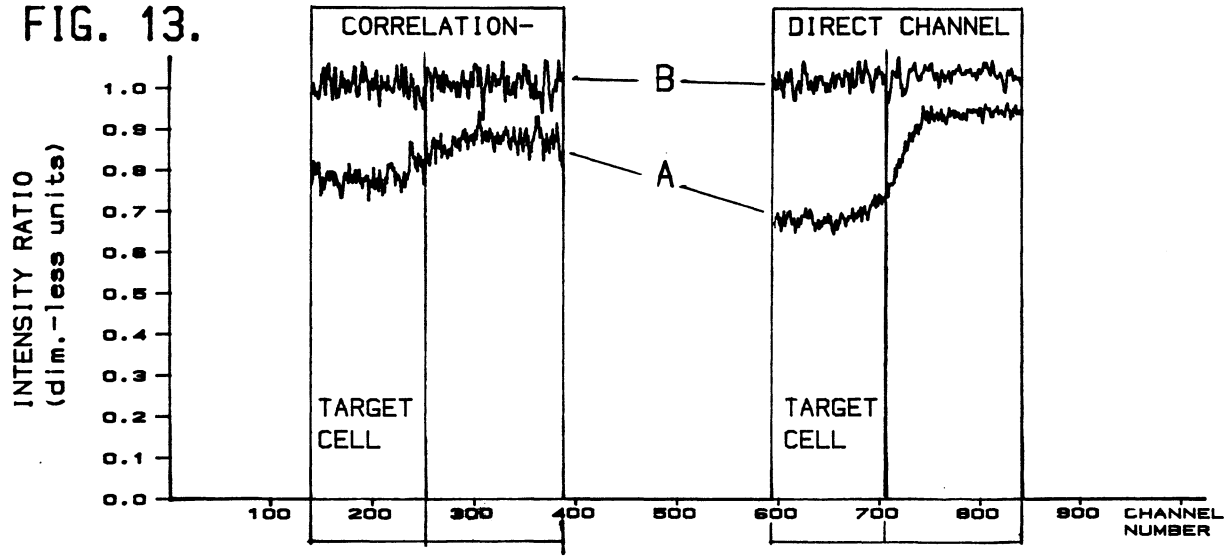

FIG. 14.

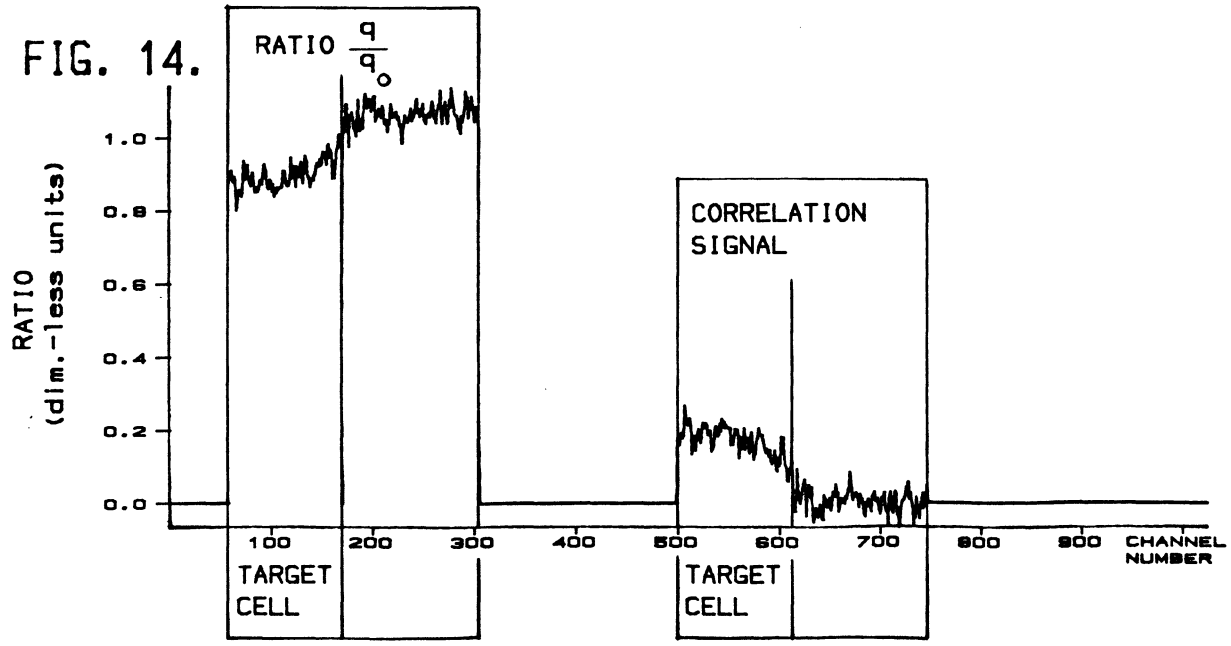

FIG. 15.
[Ref. 20.]

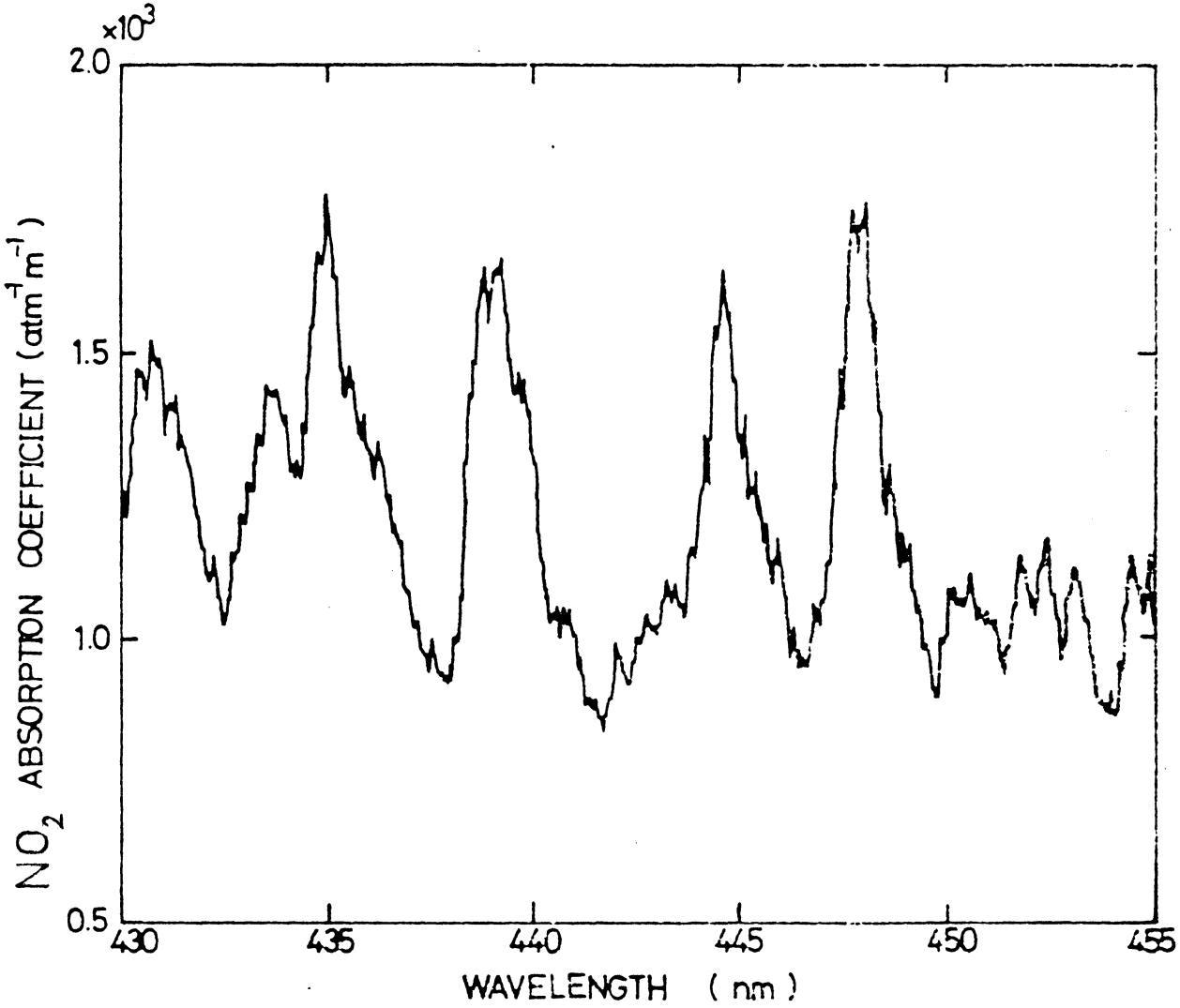
×10³
2.0
1.5
1.0
0.5
NO₂ ABSORPTION COEFFICIENT (atm⁻¹m⁻¹)
430
435
440
445
450
455
WAVELENGTH (nm)

NO_2 MEASUREMENT

FIG. 16.

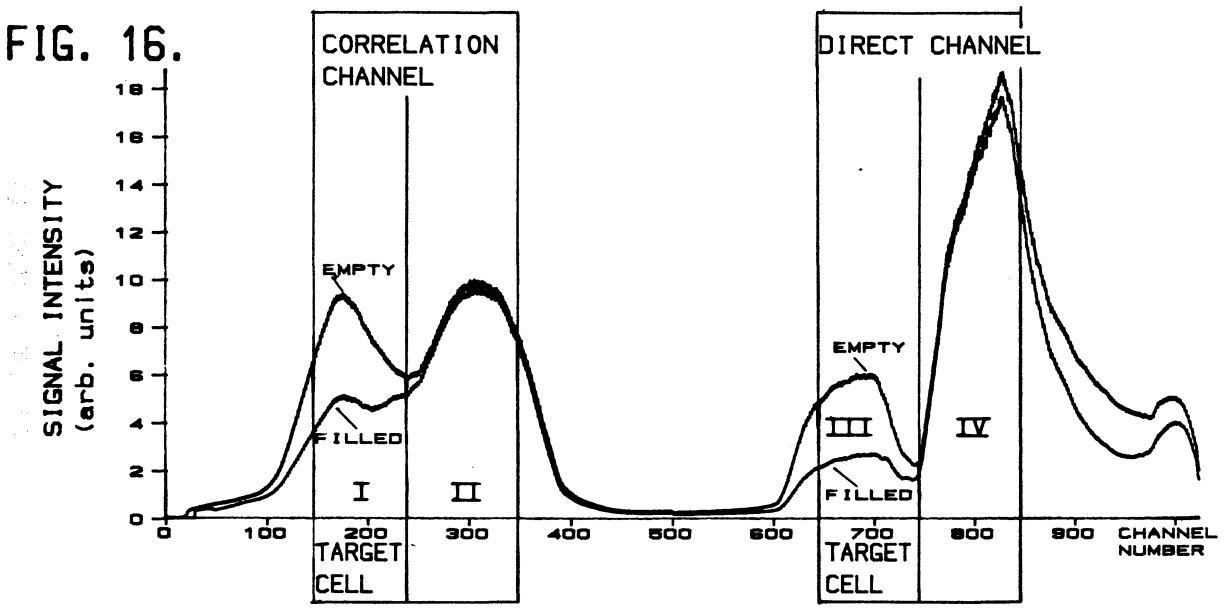

FIG. 17.

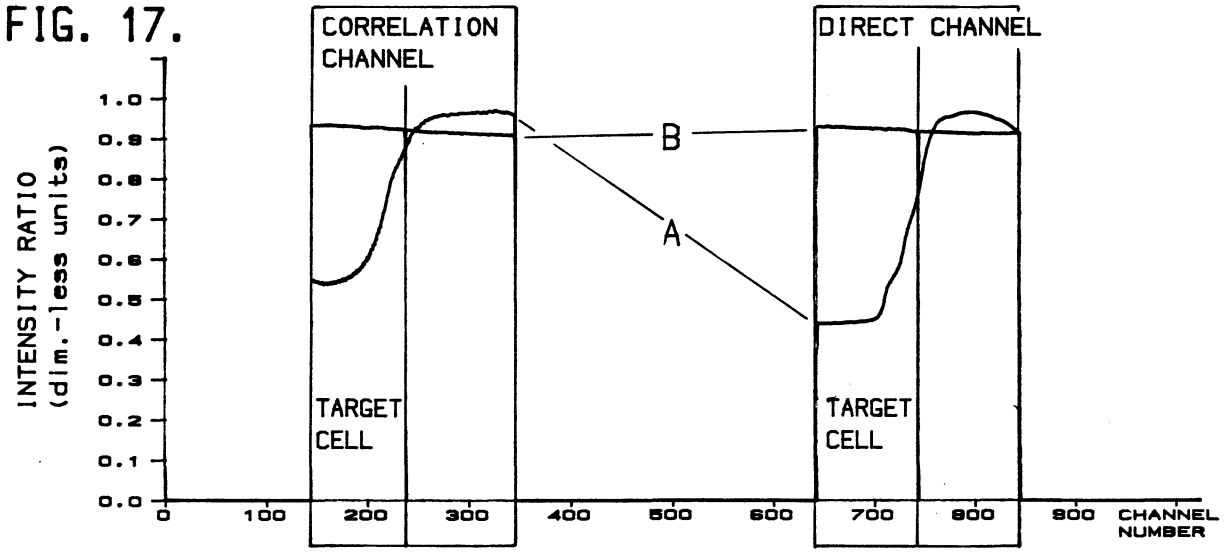

FIG. 18.

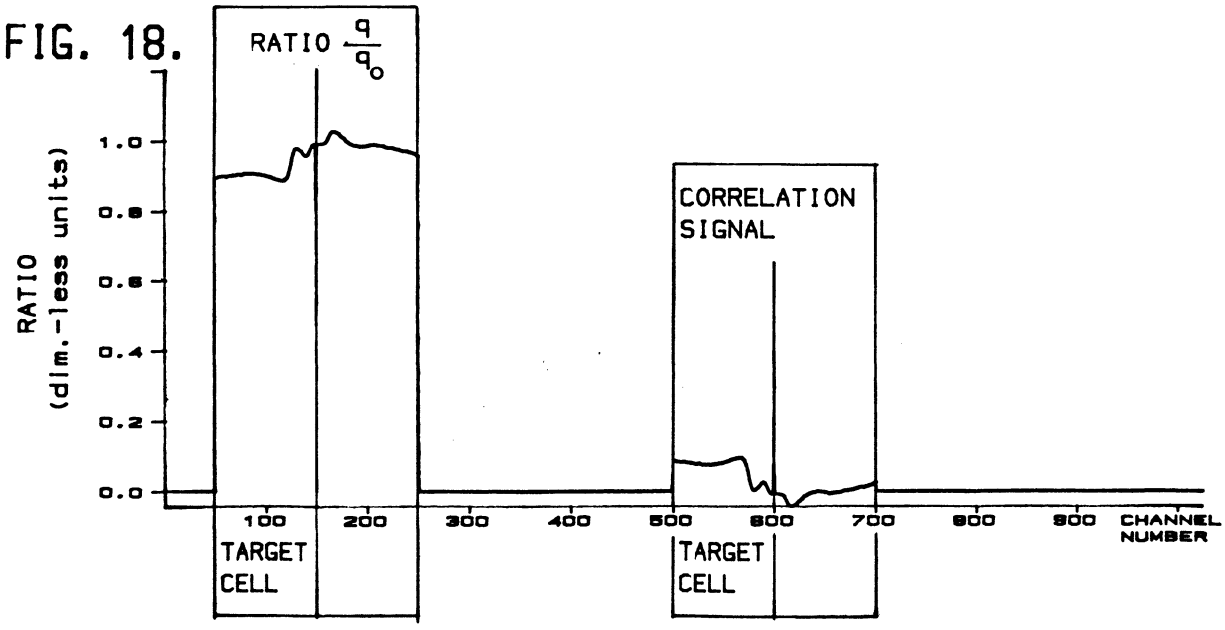

PLUME MEASUREMENT

FIG. 19.

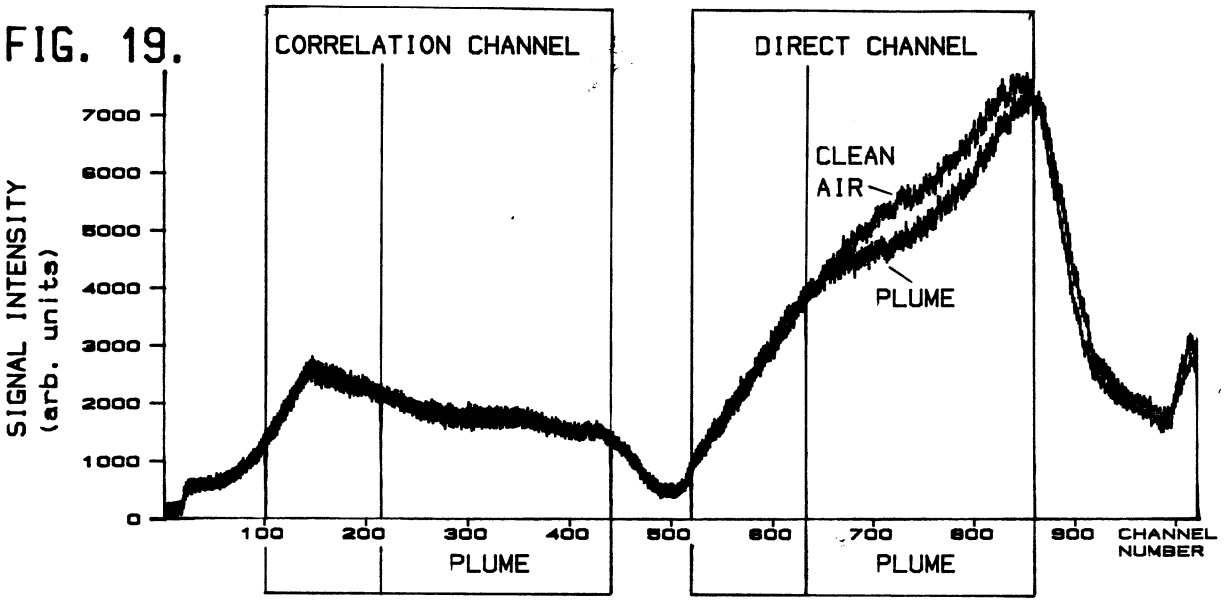

FIG. 20.

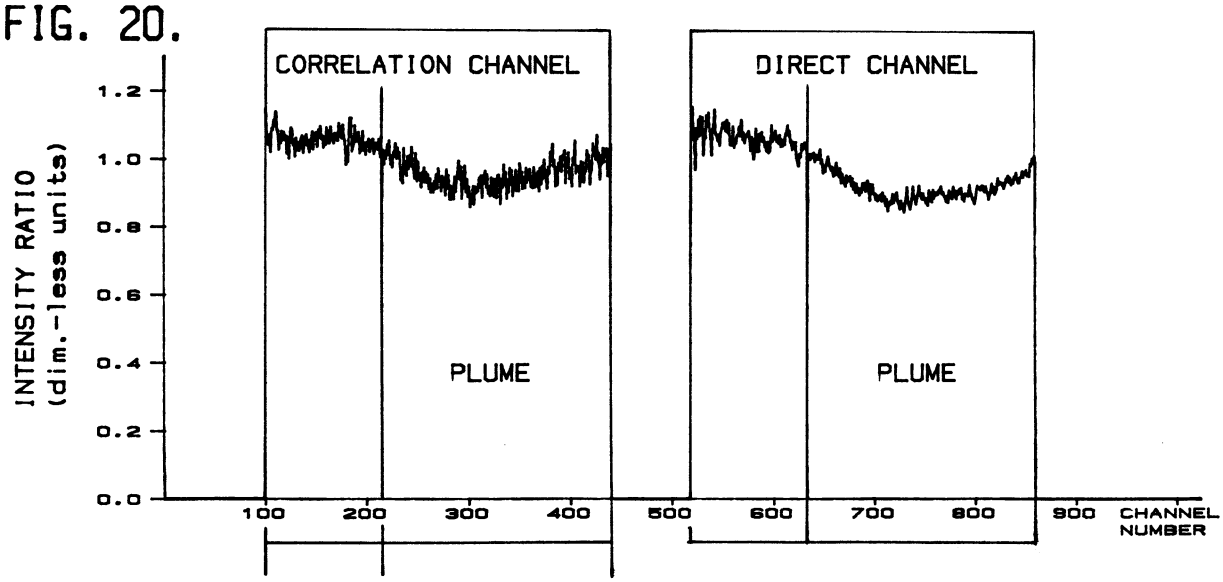

FIG. 21.

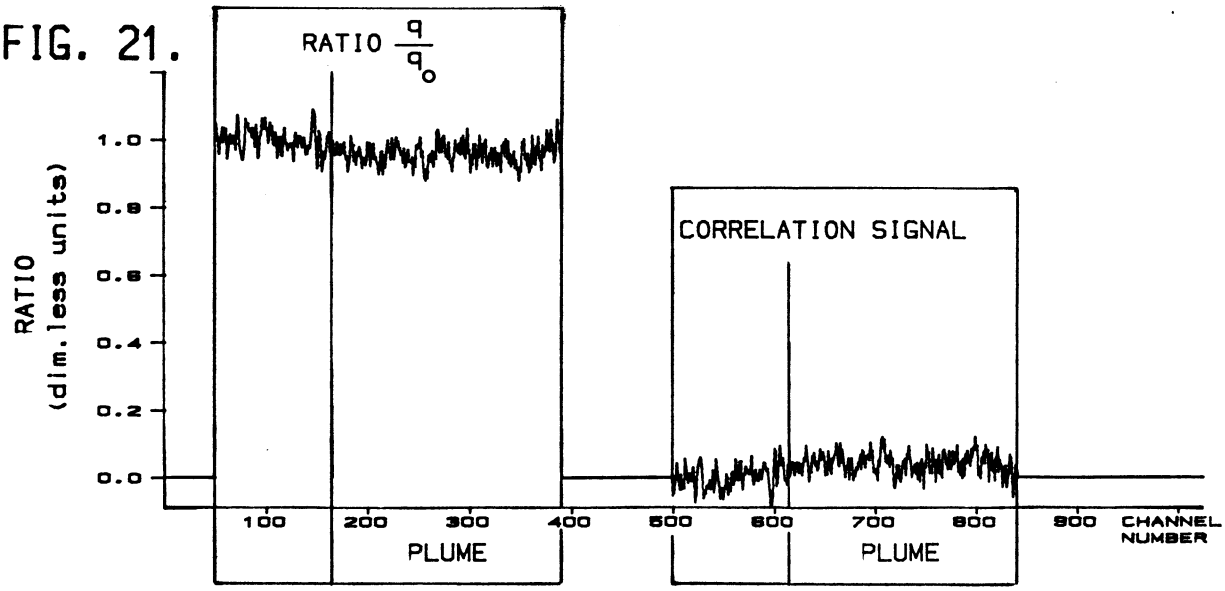

DIAGRAM I

CORRELATION SIGNAL (THEORETICAL)

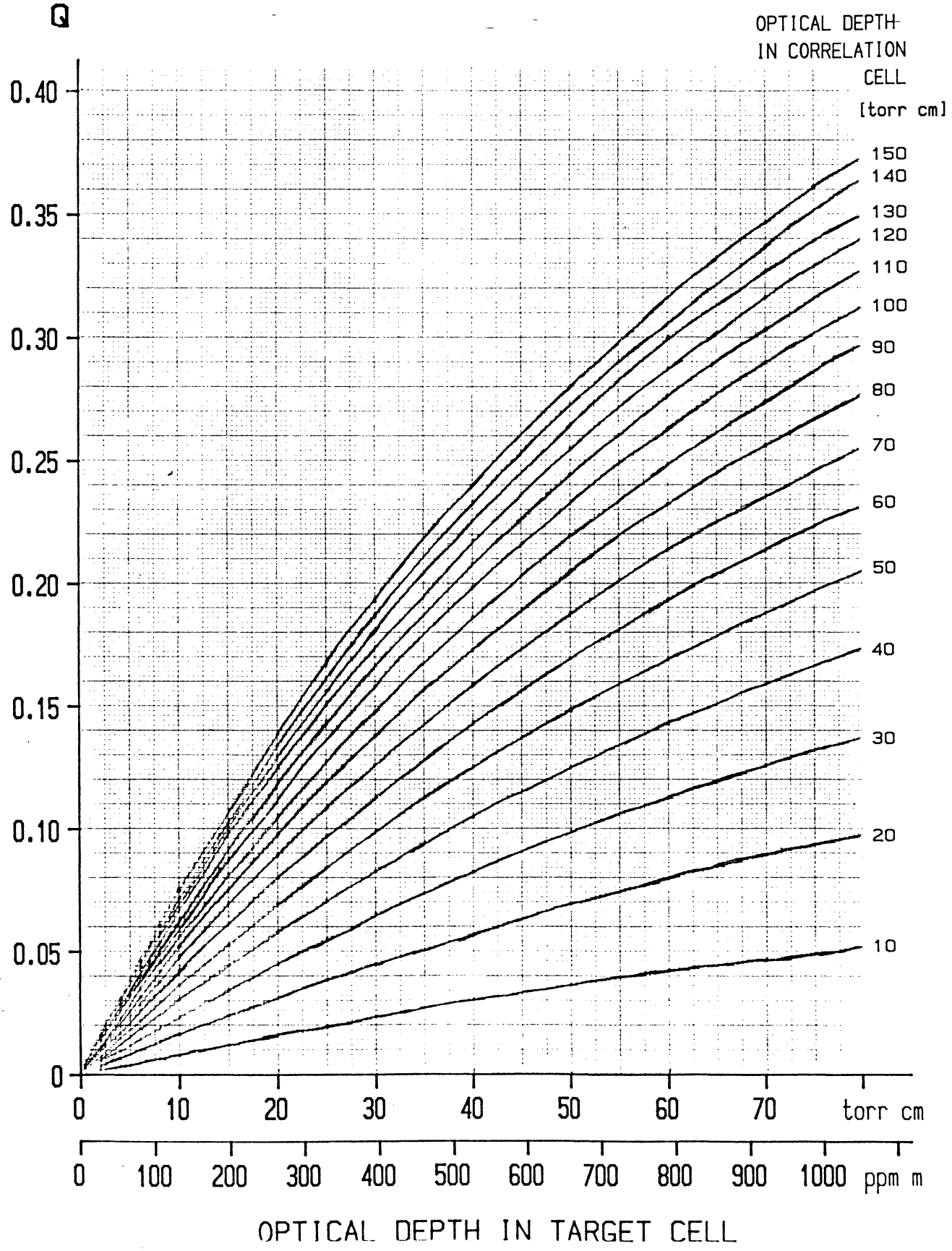

DIAGRAM II

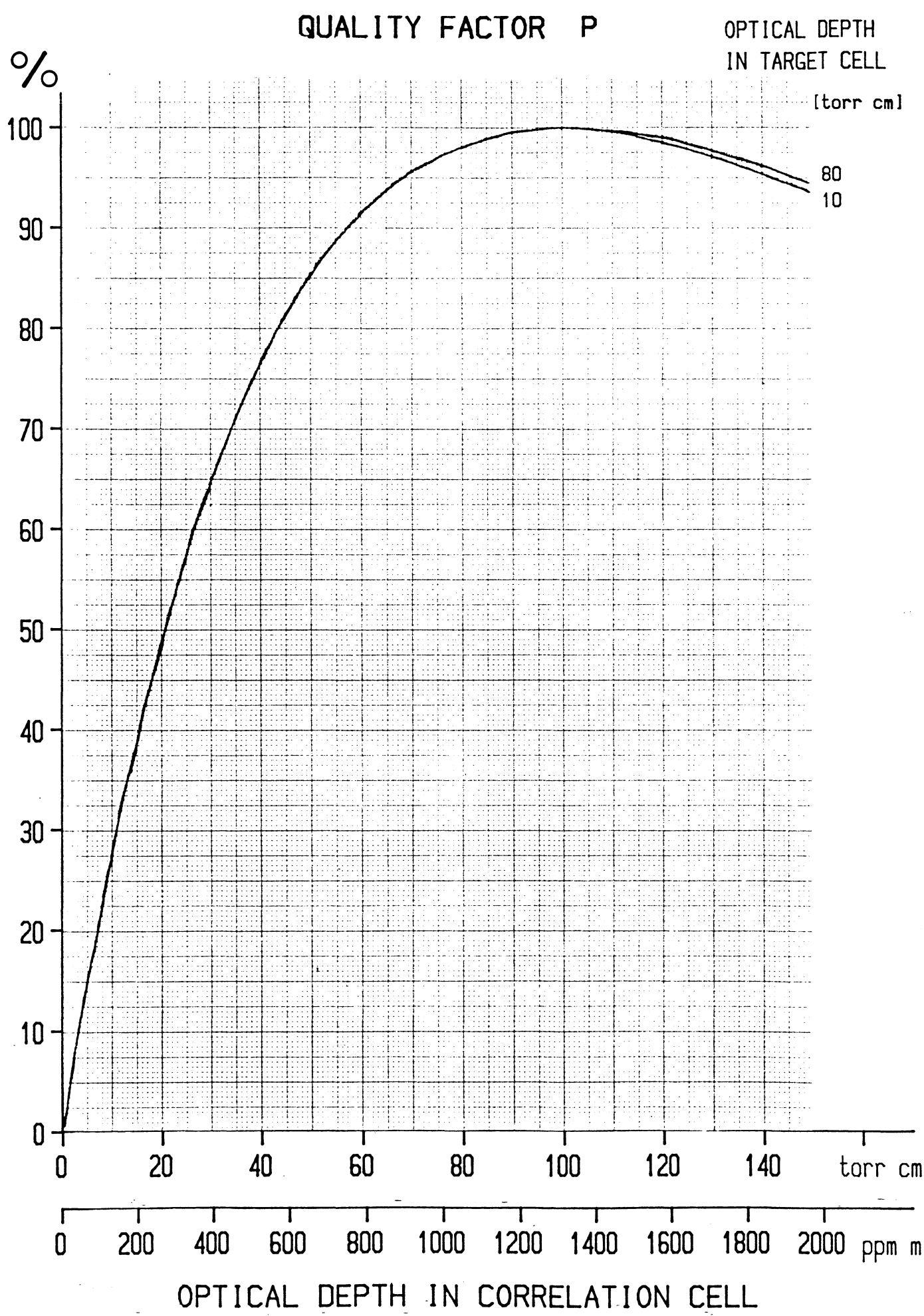
QUALITY FACTOR P
OPTICAL DEPTH
IN TARGET CELL
[torr cm]
%
100
90
80
70
60
50
40
30
20
10
0
80
10
0
20
40
60
80
100
120
140
torr cm
0
200
400
600
800
1000
1200
1400
1600
1800
2000
ppm m
OPTICAL DEPTH IN CORRELATION CELL

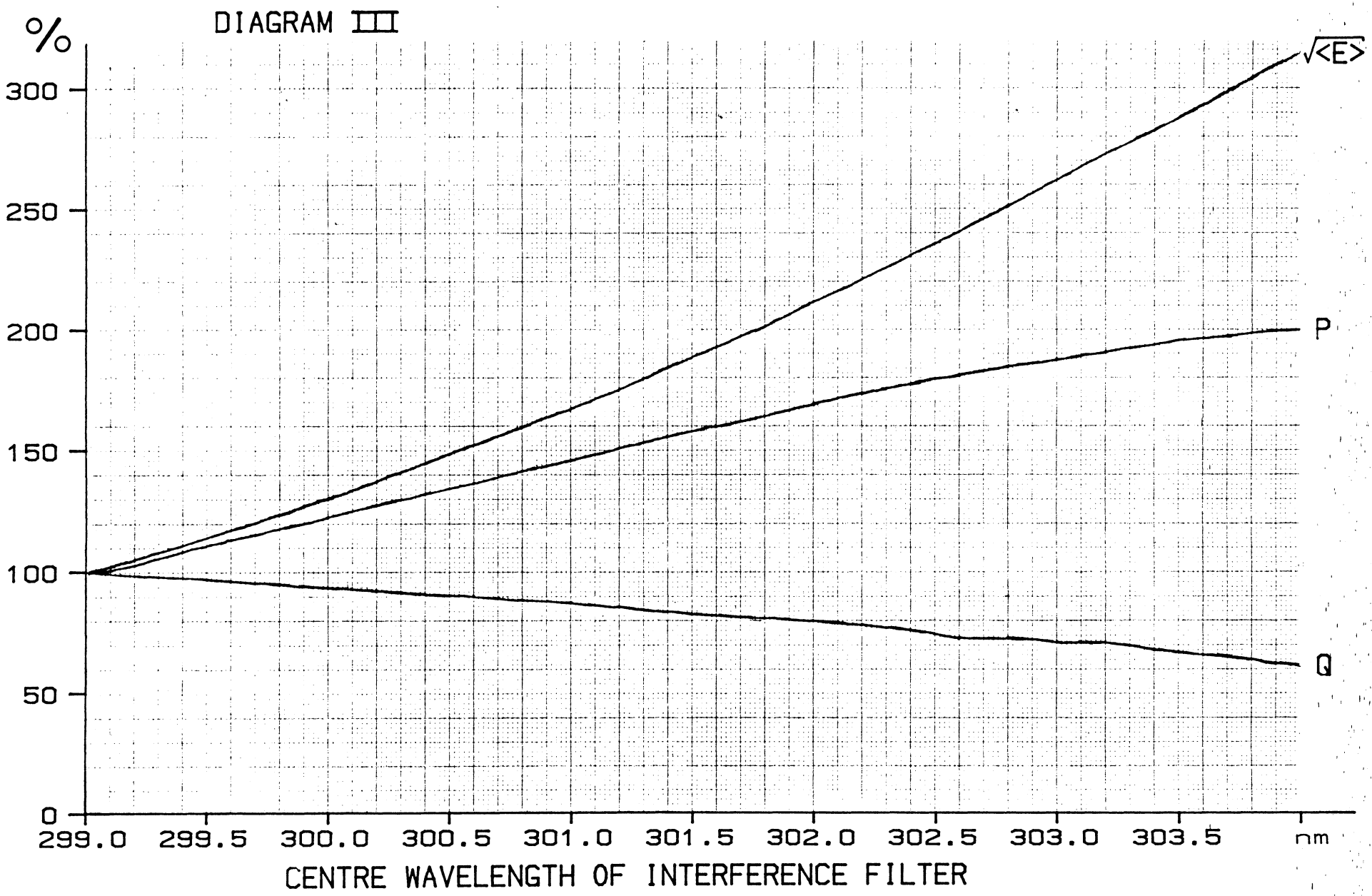
DIAGRAM III
%
300
250
200
150
100
50
0
√<E>
P
Q
299.0
299.5
300.0
300.5
301.0
301.5
302.0
302.5
303.0
303.5
nm
CENTRE WAVELENGTH OF INTERFERENCE FILTER

DIAGRAM IV

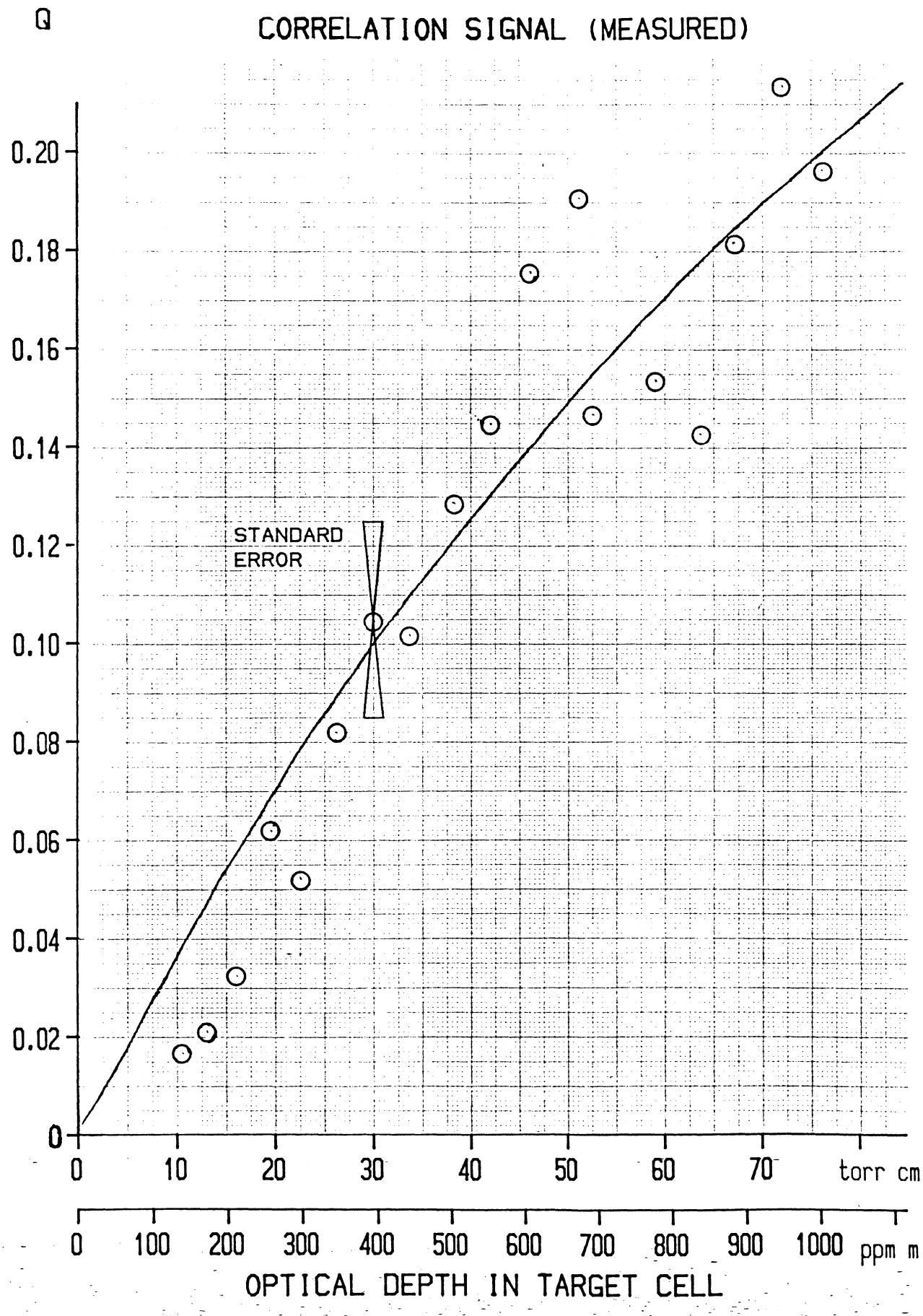
Q
CORRELATION SIGNAL (MEASURED)
0.20
0.18
0.16
0.14
0.12
0.10
0.08
0.06
0.04
0.02
0
STANDARD
ERROR
0
10
20
30
40
50
60
70
torr cm
0
100
200
300
400
500
600
700
800
900
1000
ppm m
OPTICAL DEPTH IN TARGET CELL